JOSA COMMUNICATIONS

The JOSA Communications section is for short papers reporting new results that are deemed to be especially significant or of wide interest. A Communication must be no longer than four printed pages, including title and abstract. Page proofs are provided to authors.

Characterization of a continuous-wave Raman laser in H_2

J. K. Brasseur, P. A. Roos, K. S. Repasky, and J. L. Carlsten

Department of Physics, Montana State University, Bozeman, Montana 59717

Received April 8, 1999; revised manuscript received April 9, 1999

We present a time-dependent theory that describes the continuous-wave (cw) Raman laser in H_2. The time-dependent theory is compared with existing theories, and threshold measurements are taken. The relative intensity noise of the pump and the Stokes beams is measured and found to be in agreement with the predictions of the presented theory. The Raman laser decreases the relative intensity noise of the pump beam by 34 dB/Hz at a frequency of 30 kHz. In addition, the spectral heterodyne beat-note linewidth of the continuous-wave Raman laser is measured to be 8 kHz. © 1999 Optical Society of America [S0740-3224(99)01908-6]

OCIS codes: 140.3550, 190.5650, 290.5910, 290.5860.

1. INTRODUCTION

Recent experimental[1,2] and theoretical[2,3] studies have been conducted in nonresonant Raman scattering with a continuous-wave (cw) laser pump source. These studies have been made possible by developments in mirror-coating technology that have led to the availability of low-loss, high-reflectivity mirrors. With reflectivities approaching 99.995% for multiple wavelengths, high-finesse cavities (HFC's) can be constructed with finesses of 50,000 and higher.[4,5] When resonant, the circulating power inside a HFC is roughly the finesse times the optical power at the entrance of the cavity. Thus stimulated Raman scattering can be studied with relatively low-power cw lasers.

Raman scattering occurs when an incident photon interacts with a molecule (or an atom) and generates a red-shifted photon (Stokes) resulting from the conservation of energy when the excitation in the molecule occurs. The molecular excitation can be vibrational, rotational, or electronic. In Refs. 1–3 nonresonant vibrational Raman scattering in H_2 was studied, and thresholds of the order of a milliwatt were observed. With low-cost diode lasers, cw Raman lasers covering the spectrum from the visible to the near IR ($\sim$4 μm) are possible.

Possible applications of the cw Raman laser will be in laser frequency synthesis and high-resolution spectroscopy. Two attributes that were not discussed in Refs. 1–3 but are critical to the applicability of the source are its spectral purity and amplitude noise. In this paper we address the amplitude noise of the cw Raman laser both experimentally and theoretically. In addition, the spectral linewidth and stability of the source are measured.

This paper is organized in the following manner. Section 2 develops the time-dependent cw Raman laser equations. Section 3 examines the steady-state limits of these equations and compares the results with previous theories. Section 4 solves the time-dependent equations to predict the temporal dynamics of the cw Raman laser as seen by relaxation oscillations as well as the relative intensity noise (RIN). Section 5 provides the experimental verification of the time-dependent theory. Section 6 studies the free-running linewidth of the cw Raman laser. Section 7 contains some concluding remarks, and Appendix A is provided to discuss the particular difficulties in phase and frequency locking of the pump laser to the Raman cavity as a result of the Raman process.

2. TIME-DEPENDENT RAMAN LASER EQUATIONS

Theoretical studies were conducted that predicted the effects of using a nonclassical pump source for a nonresonant cw Raman laser.[6] These studies predicted that a photon-number squeezed pump source would produce a photon-number squeezed Stokes output. In addition, preliminary theoretical studies were performed on a cw Raman laser in H_2.[2,3,7] However, the theories presented in Refs. 2, 3 and 7 are steady-state theories that lack the time dependence to predict the relaxation oscillations seen at high pump powers in Refs. 1 and 2.

Behavior seen in a quasi-cw Raman laser in NH_3 has been described mathematically.[8] Using the equations derived in Ref. 8 with the additional assumptions that the time rate of change of the population is zero and the coherence between the ground and the vibrational state is well established,[9] we arrive at an equation that describes the growth of the Stokes field. However, the assumption that the pump field is not depleted is no longer valid, so a pump equation also needs to be included. This is done by a method similar to that outlined in Refs. 2 and 8, with optical pumping phenomenologically added. To simplify the equations further, the pump and the Stokes fields are

assumed to be resonant with the optical cavity. As a result, we have the following time-dependent equations that describe fields inside the Raman laser cavity:

$$\dot{E}_p = -L_p E_p - \frac{\omega_p}{\omega_s} G|E_s|^2 E_p + K(E_{p_{\text{in}}}, t), \tag{1}$$

$$\dot{E}_s = -L_s E_s + G|E_p|^2 E_s. \tag{2}$$

$E_p(E_s)$ is the pump (Stokes) field, and $\omega_p(\omega_s)$ is the pump (Stokes) frequency. The losses that are due to the mirrors at the pump (Stokes) frequency are given by $L_p(L_s)$. The gain of the Raman system is given by G, and the cavity is optically pumped by $K(E_{p_{\text{in}}}, t)$, where $E_{p_{\text{in}}}$ is the pump field incident upon the HFC. The Raman gain G for the Stokes field is[10]

$$G = \frac{1}{2}\left[\frac{1}{8}\alpha c\left(\frac{\epsilon_0}{\mu_0}\right)^{1/2}\right]\left(\frac{2\lambda_p}{\lambda_p + \lambda_s}\right), \tag{3}$$

where α is the plane-wave gain coefficient, c is the speed of light, and $2\lambda_p/(\lambda_p + \lambda_s)$ is a mode-filling parameter that accounts for the focusing of the beams, where $\lambda_{p(s)}$ is the wavelength of the pump (Stokes) beam.[11] A standing wave is formed inside the HFC instead of a traveling wave; so a spatial average was performed that reduced the gain by a factor of 2.[12] By setting G and $K(\omega, t)$ equal to zero in Eqs. (1) and (2), we arrive at the following expression for mirror losses L_p and L_s:

$$L_{p(s)} = -\frac{c}{2l}\ln\sqrt{R_{p(s)_f} R_{p(s)_b}}, \tag{4}$$

where l is the length of the cavity and $R_{p(s)_{f(b)}}$ is the reflectivity of the front (back) mirror at the pump (Stokes) wavelength. To determine the optical-pumping constant, $K(E_{p_{\text{in}}}, t)$, we set the gain, G, equal to zero in Eq. (1). We then solve the inhomogeneous differential equation with the appropriate boundary conditions. This results in the $K(E_{p_{\text{in}}}, t)$ constant's taking the following form[13]:

$$K(E_{p_{\text{in}}}, t) = \frac{c}{l}\sqrt{T_{p_f}} E_{p_{\text{in}}}, \tag{5}$$

where the transmission of the front mirror at the pump wavelength, T_{p_f}, is needed to let us write Eq. (5) in terms of $E_{p_{\text{in}}}$. Figure 1 shows the results of numerically integrating the Raman laser equations (1) and (2).[14] The pump field inside the cavity increases with time until the threshold of the Raman laser is reached. The Stokes field then grows, and a relaxation oscillation is observed that is damped rapidly. The steady-state values for the pump and the Stokes fields are then reached.

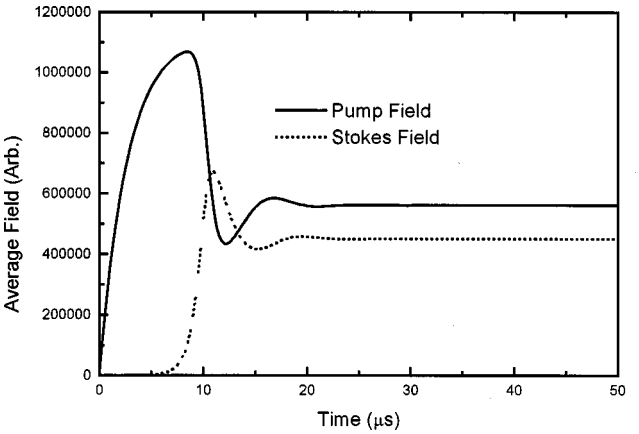

Fig. 1. Growth of the pump (solid curve) and the Stokes (dotted curve) fields shown as a function of time. A relaxation oscillation occurs at ~12 μs but is damped out in one oscillation.

3. STEADY-STATE LIMIT OF RAMAN LASER EQUATIONS

In the steady state, Eqs. (1) and (2) are set to zero, and we solve for the pump and the Stokes fields. This results in the following expressions for the steady-state pump field $E_{p_{\text{ss}}}$ and the Stokes field $E_{S_{\text{ss}}}$ inside the Raman cavity:

$$E_{p_{\text{ss}}} = (L_S/G)^{1/2}, \tag{6}$$

$$E_{S_{\text{ss}}} = \left[\frac{\omega_S(K - L_p E_p)}{\omega_p G E_p}\right]^{1/2}. \tag{7}$$

Equation (6) is independent of the pumping constant K; so, once the cw Raman laser threshold is reached, the pump power inside the HFC remains constant. The threshold occurs when the Stokes field amplitude becomes real valued ($K = L_p E_p$). Using Eqs. (5)–(7), we can express the required pump field incident upon the Raman cavity for threshold as

$$E_{p_{\text{in,thres}}} = \frac{lL_p}{c}\left(\frac{L_S}{T_{p_f} G}\right)^{1/2}. \tag{8}$$

To find the fields outside the Raman cavity we multiply by $(1/2)\sqrt{T}$, since light can escape from either of two mirrors. The fields exiting the HFC therefore take the following forms:

$$E_{p_{\text{ssf}}} = -\sqrt{R_{p_f}} E_{p_{\text{in}}} + {}^1/_2\sqrt{T_{p_f}} E_{p_{\text{ss}}}, \tag{9a}$$

$$E_{p_{\text{ssb}}} = {}^1/_2\sqrt{T_{p_b}} E_{p_{\text{ss}}}, \tag{9b}$$

$$E_{S_{\text{ssf}}} = {}^1/_2\sqrt{T_{S_f}} E_{S_{\text{ss}}}, \tag{10a}$$

$$E_{S_{\text{ssb}}} = {}^1/_2\sqrt{T_{S_b}} E_{S_{\text{ss}}}, \tag{10b}$$

where the first term on the right-hand side of Eq. (9a) accounts for the reflected incident pump field. While expressions (9) and (10) do not explicitly show a dependence on absorption and scattering losses, the expressions do depend on the R (reflectivity) and the T (transmission) of the mirrors, and these values must satisfy $R + T + A = 1$. Thus the absorption dependence is implicit in the expressions.

The pump and the Stokes fields can be converted into powers by the following equation:

$$\Pi = \frac{1}{2}\left(\frac{\epsilon_0}{\mu_0}\right)^{1/2}|E|^2 A, \tag{11}$$

with the scaled area A for both the pump and the Stokes fields given by[11,15]

$$A = \frac{l\lambda_p}{4\tan^{-1}(l/b)}, \tag{12}$$

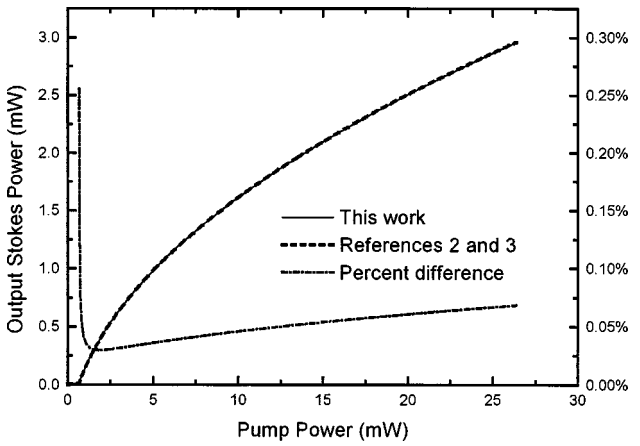

Fig. 2. Comparison of the predictions of Ref. 2 and 3 (dashed curve) with the steady-state limit of the presented time-dependent theory (solid curve). The percent difference of the theories is plotted (dashed–dotted curve). On average the theories differ by less than 1 part per 1000.

where l is the length of the cavity and b is the confocal parameter of the beam. Figure 2 shows the predictions of Eqs. (9) and (10) with the predictions of Refs. 2 and 3 overlaid.[14] We see that the steady-state predictions of the current theory are in good agreement with previous steady-state theories.

4. RELAXATION OSCILLATIONS AND RELATIVE INTENSITY NOISE

Figure 1 shows the relaxation oscillation damping out in the absence of noise to drive the oscillation. To show the effect of intensity noise on the output of the cw Raman laser, a noise term is added into Eq. (1), giving the following modified cw Raman laser equations:

$$\dot{E}_p = -L_p E_p - \frac{\omega_p}{\omega_S} G|E_S|^2 E_p + K[1 + \beta \sin(\omega t)], \quad (13)$$

$$\dot{E}_S = -L_S E_S + G|E_p|^2 E_S, \quad (14)$$

where ω is the angular frequency of the noise and β is the amplitude of the oscillation relative to the incident pump field. These equations are numerically integrated for various pump powers and angular noise frequencies, allowing calculation of the amplitude noise.

The amplitude noise of a laser is commonly expressed in terms of RIN. Noise predicted by Eqs. (13) and (14) is converted into RIN according to the following equation:

$$\mathrm{RIN}_{\mathrm{output}} = 40 \log_{10}\left(\frac{\delta E_{\mathrm{rms}}}{E_{\mathrm{ss}}}\right), \quad (15)$$

where δE_{rms} is the field rms noise and E_{ss} is the steady-state value of the field at the output of the cw Raman laser.

Since the HFC can add noise by converting frequency deviations into intensity noise, the $\mathrm{RIN}_{\mathrm{output}}$ of the pump and the Stokes beams were normalized to the pump RIN at the exit of the HFC below threshold for measurement purposes. Thus the normalized RIN for the pump (Stokes) is given by

$$\Delta_{P(S)} = \mathrm{RIN}_{\mathrm{output}_{P(S)}} - 40 \log_{10}(\beta_{\mathrm{rms}}) - 20 \log_{10}[C_p(\omega)], \quad (16)$$

where $\beta_{\mathrm{rms}} = \beta/\sqrt{2}$ and $C_p(\omega)$ is the frequency response of the HFC for the pump beam. Therefore the normalized RIN of the pump (Stokes) beam $\Delta_{P(S)}$ allows general statements about the reduction or addition of amplitude noise by just the Raman process. The functional dependence of Δ_P and Δ_S on the noise frequency $\omega/2\pi$ is calculated with Eqs. (13)–(16).[14]

Figure 3 shows the results of this calculation for the normalized RIN of the pump (Stokes) $\Delta_{P(S)}$ for a pump power of four times the threshold of the Raman laser. The normalized RIN of the Stokes beam Δ_S is seen to increase to a noise frequency of 125 kHz, where the relaxation-oscillation frequency is reached. Furthermore, for noise frequencies above the relaxation-oscillation frequency, the response of the HFC at the Stokes wavelength reduces Δ_S. The Stokes RIN at the relaxation-oscillation frequency is seen to be 17 dB/Hz larger than the input pump RIN.

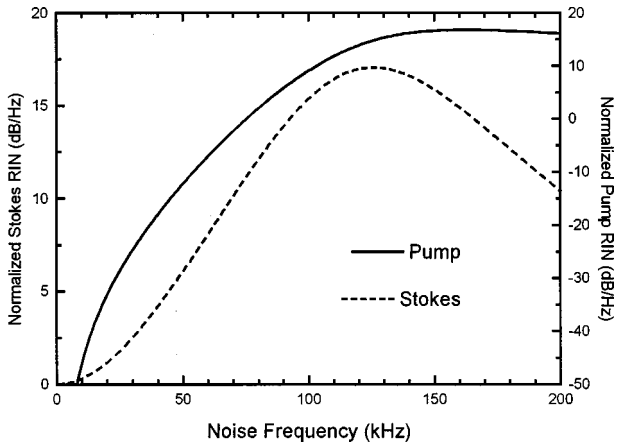

Fig. 3. Normalized RIN's of the Stokes (dashed curve) and pump (solid curve) beams are shown as a function of noise frequency at four times the threshold of the Raman laser.

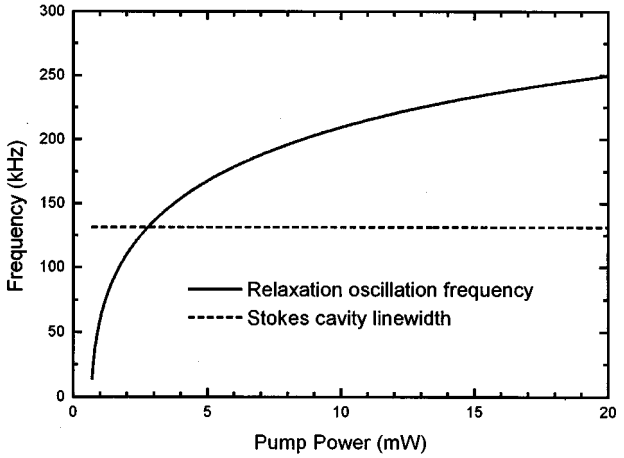

Fig. 4. Relaxation-oscillation frequency (solid curve) is shown as a function of pump power. The Stokes cavity linewidth (dashed line) is overlaid for reference. The threshold of the Raman laser is 640 μW.

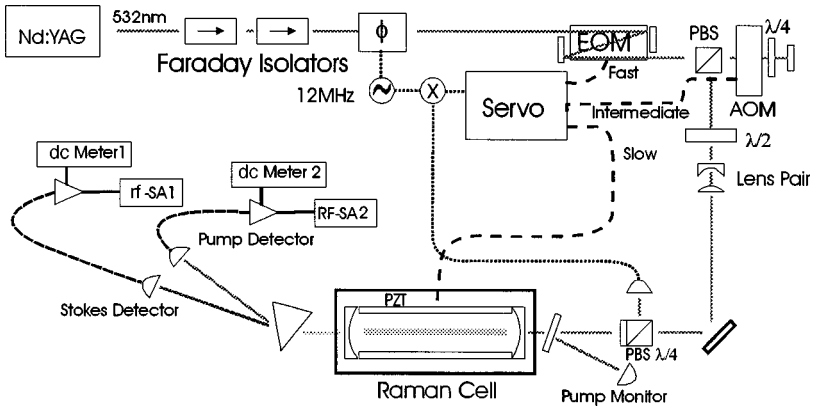

Fig. 5. Experimental apparatus used to measure the threshold and the RIN of the cw Raman laser is shown.

The calculated normalized RIN of the pump beam Δ_P is also shown in Fig. 3. Owing to the self-limiting nature of the pump beam [Eq. (6)], Δ_P is expected to decrease with respect to the input pump beam. However, the medium has a resonance that is due to relaxation oscillations, seen in Δ_S of Fig. 3, that causes an increase in Δ_P near the relaxation-oscillation resonance. Thus, for noise frequencies below the relaxation-oscillation resonance, Δ_P initially increases with the noise frequency until the relaxation oscillation is reached; then Δ_P levels off for larger noise frequencies, as shown in Fig. 3.

Figure 4 shows the calculated dependence of the relaxation-oscillation frequency on the pump power of the Raman laser. The relaxation-oscillation frequency is calculated by solution of Eqs. (13)–(16) for various pump powers and selection of the frequency corresponding to the maximum of Δ_S. The relaxation-oscillation frequency of the Raman laser is seen to increase with pump power, but the frequency increases much more slowly when it reaches the Stokes cavity linewidth. The Stokes cavity linewidth is reached at a pump power of approximately four times threshold. For large pump powers the relaxation-oscillation frequency levels off to approximately twice the Stokes cavity linewidth.

5. EXPERIMENTAL APPARATUS

Figure 5 shows the experimental apparatus used to measure the threshold and the RIN of the cw Raman laser. The device was pumped by a frequency-doubled Nd:YAG laser with output powers as great as 200 mW. The output of this Nd:YAG laser was at 532 nm and was sent through two Faraday isolators to minimize feedback to the Nd:YAG laser. The beam was then passed through a resonant phase modular to place sidebands on the carrier frequency required for phase and frequency locking of the cavity and the pump beam. An electro-optic modular (EOM) in conjunction with an acousto-optic modular (AOM) provided external phase and frequency tuning of the laser frequency.[16] A half-wave plate with a downstream polarizing beam splitter (PBS) provided a variable pump power. The beam then travelled through a two-element lens pair to mode match the pump beam to the cavity. A polarizing beam splitter in conjunction with a quarter-wave plate allowed for the monitoring of the reflected beam for phase and frequency locking. A fast photodetector was used to measure the error signal. A low-noise amplifier gave the signal 30 dB of gain before it was mixed to dc. The error signal entered the servo, which sent the slow corrections (dc, 1 kHz) to a piezoelectric transducer (PZT) used to control the spacing of the HFC mirrors. The intermediate frequencies were sent to the AOM (10–180 kHz), whereas the fast corrections were sent to the EOM (dc, 800 kHz). A small portion of the beam was diverted by a glass slide to monitor the pump power at the front of the cavity. A prism was used to separate the pump (532 nm) and the Stokes (683 nm) beams spatially at the exit of the cavity. The photodetector signals were split. For measurement of the output powers, the dc signals were sent to digital voltmeters; the ac signals (>10 Hz) were given a transimpedence gain of 30 dB, and the RIN's of the pump and the Stokes beams were measured by rf spectrum analyzers.

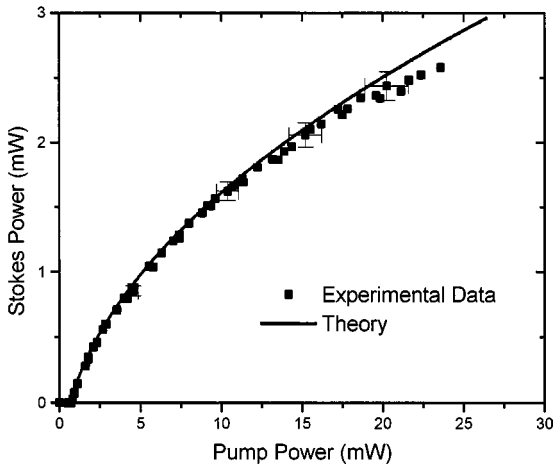

Fig. 6. Stokes output versus pump power for the cw Raman laser is shown with the theory overlaid. The threshold was measured to be 640 ± 30 μW.

Figure 6 shows the output Stokes power as a function of input pump power, and Fig. 7 shows the photon conversion efficiency as a function of pump power. The threshold of the cw Raman laser is 640 ± 30 μW,[17] and the maximum conversion efficiency is 27 ± 3% at 2.6 mW of pump power.[18] The theoretical fit was obtained with Eqs. (9) and (10) and with mirror reflectivities (transmissions) of 0.99980 [156 parts in 10^6 (ppm)] and 0.99977 (163 ppm) for the pump and the Stokes wave-

lengths, respectively.[19] The Raman cell was filled to 10 atm (7.6×10^3 Torr) with H_2, which gave a Raman linewidth of 510 MHz (FWHM).[20] The cavity length was 7.68 cm, the radius of curvature of the mirrors was 25 cm, and $\alpha = 3.45 \times 10^{-9}$ cm/W.[21] Deviations from the theoretical fits at larger pump powers may be caused by distortions in the HFC mirrors. Such distortions can result from thermal heating by the absorption of the high optical power circulating in the HFC.

Figure 8 shows the pump RIN before and after the HFC with the calculated shot-noise level for reference. The pump RIN after the HFC is larger for two reasons: The AOM steers the beam slightly, which changes the coupling efficiency, and the HFC converts frequency noise into amplitude noise. Thus we normalize the pump and the Stokes RIN to the pump RIN at the exit of the cavity below threshold. The pump and the Stokes RIN were measured at every data point of the threshold curve.

Figure 9 shows the normalized RIN of the Stokes and the pump beams at four times the threshold of the Raman laser. The theoretical normalized RIN fits were obtained with Eqs. (13)–(16) and the parameters of the threshold fits.[14] Both the Stokes and the pump fits are in agreement with predictions of the theory. The significant deviations in Δ_P seen in the frequency range of 0–20 kHz are caused by instabilities in the piezoelectric transducer servo. In addition, for larger pump powers (six times threshold and larger) the phase–frequency locking system prohibited consistent measurements of the RIN at

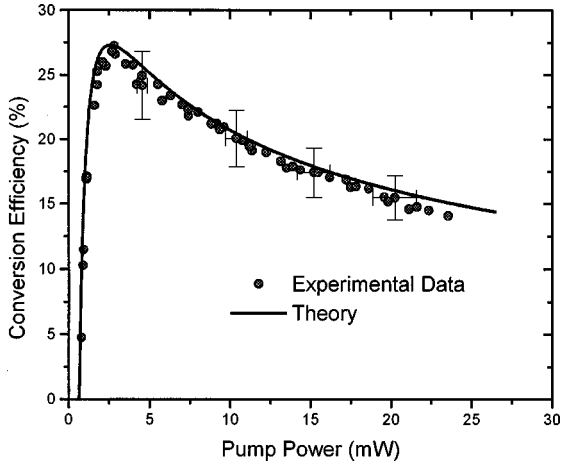

Fig. 7. Photon-number conversion efficiency versus pump power for the cw Raman laser is shown with the theory overlaid. The maximum photon-number conversion efficiency was measured to be 27 ± 3% at 2.6 mW of pump power.

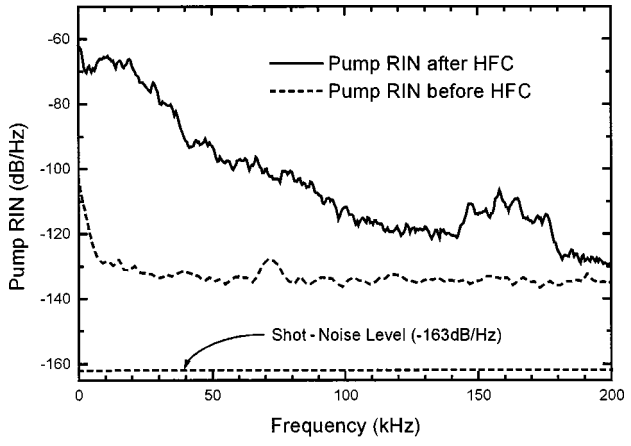

Fig. 8. RIN for the pump beam is shown before (dashed curve) and after (solid curve) the HFC as a function of frequency. The calculated shot-noise level is added for reference.

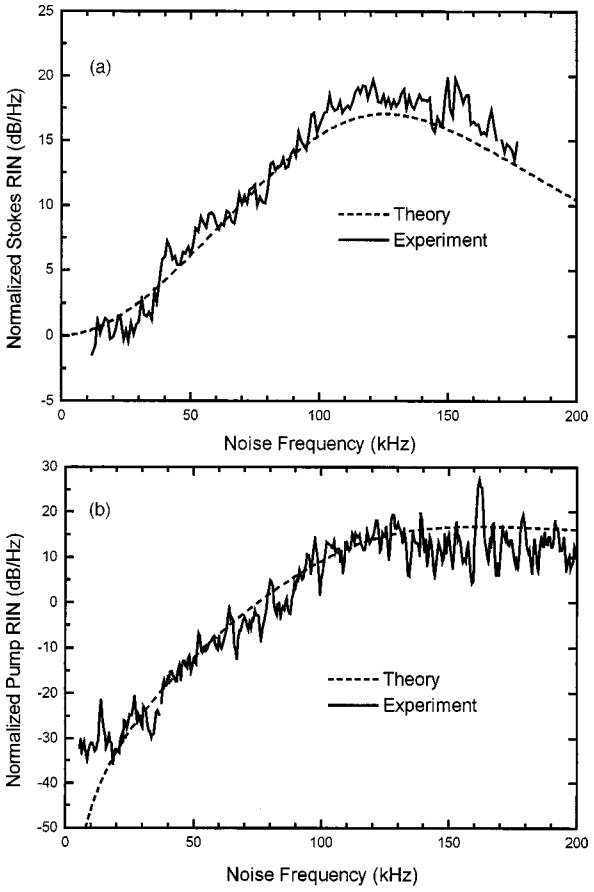

Fig. 9. (a) Normalized Stokes RIN and (b) the normalized pump RIN are shown as a function of noise frequency. Theoretical predictions of Eqs. (13)–(16) are overlaid (dashed curves).

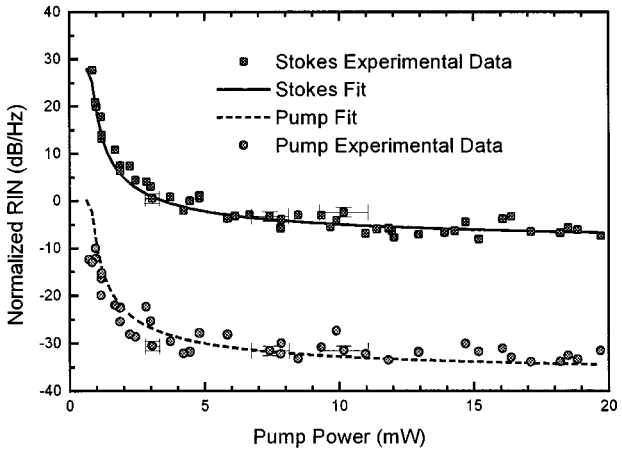

Fig. 10. Measured normalized RIN's of the pump (circles) and the Stokes (squares) beams at 30 kHz as a function of pump power is shown. The data are fitted by the time-dependent theory. The pump RIN is reduced by as much as 35 dB/Hz for higher pump powers. The threshold of the Raman laser is 640 μW.

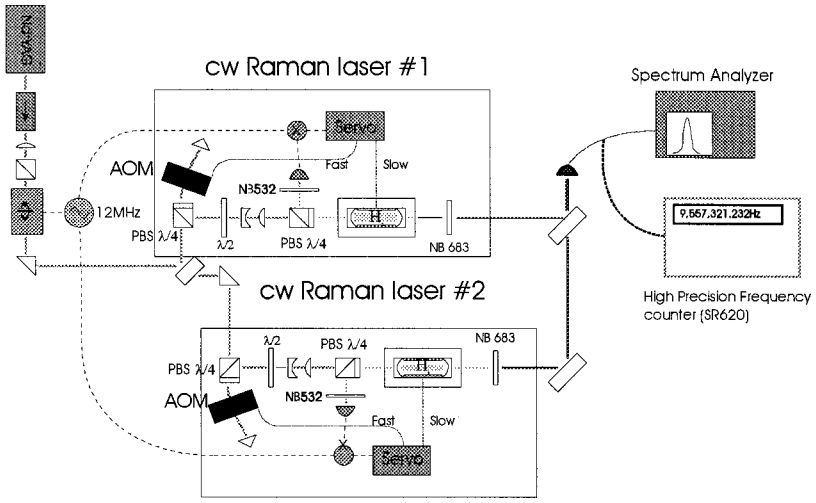

Fig. 11. Experimental apparatus used to measure the free-running linewidth and stability of the cw Raman laser is shown. NB denotes narrow band.

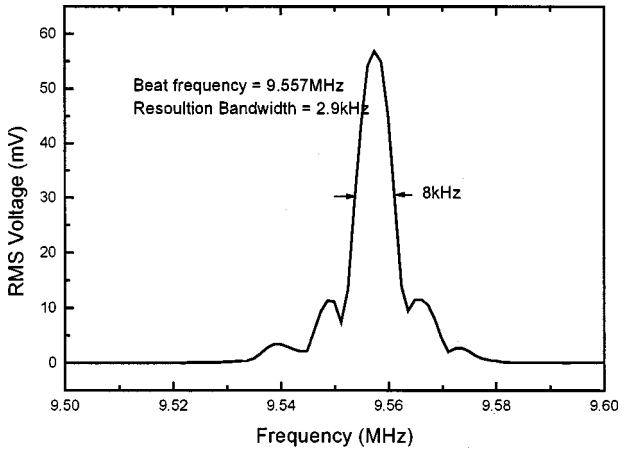

Fig. 12. Heterodyne beat-note linewidth measured by a rf spectrum analyzer. The linewidth of the cw Raman laser was measured to be 4 kHz.

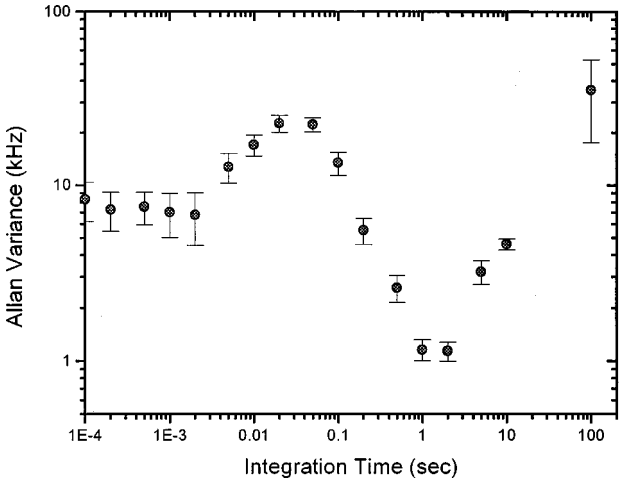

Fig. 13. Allan variance versus integration time is shown. A peak that is due to table vibrations is seen to occur at ~100 Hz.

frequencies above the pump cavity half-width (64 kHz). Appendix A addresses the difficulties in phase–frequency locking at these high pump powers.

Figure 10 shows the normalized RIN of the pump and the Stokes beams at a frequency of 30 kHz as a function of pump power. For small pump powers the normalized RIN for the Stokes was 30 dB/Hz and was reduced to −5 dB/Hz at higher pump powers. The normalized pump RIN was reduced to −34 dB/Hz for large pump powers, which was 45 dB/Hz above the calculated shot-noise level. The theoretical RIN fits were obtained with Eqs. (13)–(16) and the parameters of the threshold fits.[14] The fits show that the predictions of the theory for frequencies below the cavity half-width (64 kHz) are valid for all pump powers.

6. cw RAMAN LASER LINEWIDTH

Two identical cw Raman lasers were constructed to measure the free-running laser linewidth of the device. A simplified experimental diagram is shown in Fig. 11. The locking servo was identical to that of Fig. 5; however, the EOM for phase control was absent.[22] Emissions from the two Raman lasers were overlapped, and a rf spectrum analyzer and a precision frequency counter measured the beat signal. Figure 12 shows the spectrum analyzer output for a 10 ms sweep. The FWHM of the beat signal was measured to be 8 kHz in a resolution bandwidth of 2.9 kHz. The Schawlow–Townes laser linewidth is ~10 mHz for the cw Raman laser. Deviations from this limit were caused by vibrations experienced by the HFC[23] and were not due to the Raman process. Thus, for a well-isolated HFC, the cw Raman laser beat-note linewidth should reach the 10–100 Hz level.

The stability of the cw Raman laser was studied by measurement of the Allan variance. The Allan variance of the beat frequency shown in Fig. 13, which was calculated for a sample size of 100 for integration times of 10 s or smaller, had a sample size of 20 for the 100-s integration time. The Allan variance had a peak at ~100 Hz, caused by vibrations present on the optical table.[23] The Allan variance had a minimum of 1 kHz at an integration of ~1 s before long-term cavity drifts took over.

7. CONCLUSIONS

The threshold of the cw Raman laser was measured to be $640 \pm 30\,\mu$W. A time-dependent theory that describes the cw Raman laser was presented. The steady-state limit of the theory agrees well with existing theories. The theory also predicts the relaxation oscillations observed in Refs. 1 and 2. The theory predicts the structure of the RIN for both the pump and the Stokes beams, which is in agreement with experimental results. The heterodyne beat-note linewidth was measured to be 8 kHz in a resolution bandwidth of 2.9 kHz.

APPENDIX A: PHASE/FREQUENCY STABILITY REQUIREMENTS

To construct the stable, low-amplitude-noise cw Raman laser described in this paper, the following two criteria had to be met. The servo bandwidth needed to be larger than the HFC linewidth, owing to intensity-dependent changes of the index of refraction associated with the Raman process, and the amount of dc gain needed to be larger than expected, owing to the self-limiting nature of the pump intensity inside the HFC.

For the high pump and the Stokes intensities inside the HFC, intensity-dependent changes in the index of refraction occur. This index change affects the phase of the reference beam created by the HFC used in optical locking, so that oscillations in the pump or the Stokes beams create oscillations in the error signal. Relaxation oscillations, which occur at frequencies at or slightly larger than the cavity linewidth, are the predominant source for intensity noise for the cw Raman laser. If the bandwidth of the servo controlling the system is smaller than the cavity linewidth, the relaxation oscillation is actually driven by the control electronics. Therefore the bandwidth of the servo needed to be larger than the cavity linewidth for the relaxation oscillations to be reduced to the predictions of the theory.

The self-limiting nature of the pump intensity inside the HFC once the Raman laser lases presents an additional locking difficulty. The noise of a laser is traditionally separated into two regimes: frequency noise (noise slower than the HFC half-width) and phase noise (noise faster than the HFC half-width). As the pump rate of the Raman laser increases, so does the size of the error signal in the phase regime. However, the error signal in the frequency regime remains constant owing to the self-limiting. Traditionally, when a laser is locked to a reference cavity, the gain of the servo (feedback) is increased until instability arises, then the gain is reduced slightly. For the Raman process the instability occurs in the phase regime of the noise, so as the pump rate is increased, the gain of the servo must be decreased to maintain closed-loop stability. However, the reduction of the gain from the servo decreases the error signal in the frequency regime, reducing the long-term frequency stability of the Raman laser. This effect becomes significant for larger pump rates; for example, when the Raman laser is operated at ten times threshold, the dc gain is reduced by 20 dB. A solution is to add more dc gain below the cavity linewidth by means of a compensated integrator with a corner inside the cavity half-width.

ACKNOWLEDGMENTS

This work is supported by National Science Foundation grant PHY-9731602. We thank Jan Hall and his group at JILA and Michael Jefferson at IBM for their help.

The authors can be reached at the address on the title page or by e-mail at carlsten@physics.montana.edu.

REFERENCES AND NOTES

1. J. K. Brasseur, K. S. Repasky, and J. L. Carlsten, Opt. Lett. **23**, 367 (1998).
2. K. S. Repasky, J. K. Brasseur, L. Meng, and J. L. Carlsten, J. Opt. Soc. Am. B **15**, 1667 (1998).
3. K. S. Repasky, L. Meng, J. K. Brasseur, J. L. Carlsten, and R. C. Swanson, J. Opt. Soc. Am. B **16**, 717 (1999).
4. K. S. Repasky, L. E. Watson, and J. L. Carlsten, Appl. Opt. **34**, 2615 (1995).
5. K. S. Repasky, J. G. Wessel, and J. L. Carlsten, Appl. Opt. **35**, 609 (1996).
6. S. Rebic, A. S. Parkins, and D. F. Walls, Opt. Commun. **156**, 426 (1998).
7. P. Peterson, A. Gavrielides, and M. P. Sharma, Opt. Commun. **160**, 80 (1999).
8. R. G. Harrison, Weiping Lu, and P. K. Gupta, Phys. Rev. Lett. **63**, 1372 (1989).
9. $\dot{D}_{13}$ and $\dot{\rho}_{31}$ from Ref. 8 are set to zero. The population difference of the ground state and the vibration state is assumed to be 1, since in 10 atm (7.6×10^3 Torr) of H_2, only $\sim$1 molecule in 10^4 of the molecules available participate in the Raman process. In addition, the Raman linewidth is of the order of 510 MHz for 10 atm of H_2, which gives a coherence decay of $\sim$2 ns, whereas the Raman cavity has a build-up time of $\sim$1–10 μs; thus coherence effects can be ignored.
10. D. C. MacPherson, R. C. Swanson, and J. L. Carlsten, IEEE J. Quantum Electron. **25**, 1741 (1989).
11. G. D. Boyd, W. D. Johnston, and I. P. Kaminow, IEEE J. Quantum Electron. **QE-4**, 203 (1969).
12. Since for our system the gain per pass of the Stokes beam is $\sim 1 \times 10^{-4}$, the gain of the system can be treated as if it were linear [$\exp(G) \rightarrow 1 + G$]; thus a spatial average of the pump's field inside the Raman laser cavity is sufficient to calculate the gain. The spatial average reduces the gain by a factor of 2. This factor of one-half is absent in Refs. 1 and 2 and should be included.
13. We have an inhomogeneous differential equation, which is solved by a linear combination of the homogeneous solution and the particular solution such that the following boundary conditions are met. At time equal to zero the pump inside the cavity is zero, and at time equal to infinity our solution limits to $\sqrt{T}/(1 - \sqrt{R})$, the result of a discrete sum of the fields inside an interferometer.
14. All the fits used the following parameters: $\lambda_{p(S)}$=532 nm (683 nm), $\alpha = 3.45 \times 10^{-9}$ cm/W, $R_{p(f)} = R_{p(b)} = 0.99980$, $R_{s(f)} = R_{s(b)} = 0.99977$, $T_{p(f)} = 156$ ppm, $l = 7.68$ cm, $\beta = 0.001$ [for Eq. (13)], $b = 18$ cm. The equations were integrated numerically by use of the Bulstoer algorithm.
15. To conserve energy the areas for the pump and the Stokes beams, used to calculate power, need to be identical and are normalized to the pump beam. The wavelength dependence of the area for the Stokes beam is included in the mode-filling parameter of Ref. 11.
16. J. L. Hall and T. W. Hänsch, Opt. Lett. **9**, 502 (1984).
17. This is the optical power that is coupled into the TEM_{00} mode of the HFC; the actual power at the entrance of the cavity was 1.1 mW.

18. The measured photon conversion efficiency is smaller than the efficiency reported in Ref. 1 owing to additional exposures to atmospheric conditions; this increases the absorption of the mirrors of the HFC.
19. The values for the pump and the Stokes mirror reflectivies were measured by a cavity ring-down. The values are $R_{p(S)} = 0.99979 \pm 0.00001$ (0.99977 ± 0.00001). The transmissions were $T_p = (153 \pm 8)$ ppm, and $T_S = (150 \pm 20)$ ppm.
20. W. K. Bischel and M. J. Dyer, Phys. Rev. A **33**, 3113 (1986).
21. The calculated value for the plane-wave gain coefficient is 2.94×10^{-9} cm/W, and the experimental values are $(2.5 \pm 0.4) \times 10^{-9}$ cm/W. [See W. K. Bischel and M. J. Dyer, J. Opt. Soc. Am. B **3**, 677 (1986).]
22. The absence of the EOM does not affect the cw Raman laser linewidth, since the narrowed pump linewidth is of the order of ~1 kHz, owing to instabilities in the HFC, and the Raman linewidth for the vibrational transition is 510 MHz. However, the HFC transforms frequency noise into amplitude noise, so that an EOM was added to increase the stability at frequencies near or above the cavity half-width for the RIN measurements.
23. Vibrations on the optical table are of the order of 30 μg_{rms}, which occur at a frequency of 90 Hz.